Chapter 9

Finite Element Analysis of Cable-Stayed Bridges with Appropriate Initial Shapes Under Seismic Excitations Focusing on Deck-Stay Interaction

Ming-Yi Liu and Pao-Hsii Wang

Additional information is available at the end of the chapter

http://dx.doi.org/10.5772/48440

1. Introduction

In the last several decades, cable-stayed bridges have become popular due to their aesthetic appeal, structural efficiency, ease of construction and economic advantage. This type of bridge, however, is light and flexible, and has a low level of inherent damping. Consequently, they are susceptible to ambient excitations from seismic, wind and traffic loads. Since the geometric and dynamic properties of the bridges as well as the characteristics of the excitations are complex, it is necessary to fully understand the mechanism of the interaction among the structural components with reasonable bridge shapes, which is used to provide the essential information to accurately calculate the dynamic responses of the bridges under the complicated excitations.

In the previous studies of bridge dynamics, the responses of a cable-stayed bridge can be categorized into global, local and coupled modes [1]. The global modes are primarily dominated by the deformations of the deck-tower system with the quasi-static motions of the stay cables; the local modes predominantly consist of the stay cable motions with negligible deformations of the deck-tower system; the coupled modes have substantial contributions from both the deck-tower system and stay cables. Since the towers are usually designed with a high rigidity to obtain an adequate efficiency of the system, the significant tower deformations do not occur in the lower modes sensitive to the ambient excitations [2]. Consequently, the coupled modes are considered to be dominated by the deck-stay interaction, while the contribution from the towers can be neglected. Numerical approaches based on the finite element method have been widely used to investigate the deck-stay interaction. The finite-element models of a cable-stayed bridge can be classified into two categories [1]: the one-element cable system (OECS), in which each stay cable is represented

by a single cable element, and the multi-element cable system (MECS), in which each stay cable is discretized into multiple cable elements.

The deck-stay interaction has attracted much attention, because it not only significantly complicates both the natural frequency and mode shape characteristics of a cable-stayed bridge, but also potentially results in the large-amplitude stay cable vibrations even under the low-level deck oscillations. In the previous literature, the deck-stay interaction is due to the linear coupling (primary resonance) [3-8, 11] or the nonlinear coupling (secondary resonance), which can be further categorized into the subharmonic resonance of order 1/2 (two-to-one resonance) [3-9] and the superharmonic resonance of order 2 (one-to-two resonance) [6, 9, 10]. The primary, two-to-one and one-to-two resonances individually result in the fact that the global modes induce the direct, parametric and angle variation excitations of the local modes. Two types of simplified models: the single cable with moving anchorage [5-7] and the cable-supported cantilever beam [3, 4, 8-11], have been presented to theoretically investigate the deck-stay interaction. To extend the results of the simplified models, the OECS and MECS models of full cable-stayed bridges based on the finite element method have been widely used to explore such coupled phenomena of real structures [1, 11-16]. By focusing on the analytical and numerical study of the linear coupling, the localization factor was introduced to reveal the frequency veering phenomenon and to evaluate the mode hybridization level of a cable-stayed bridge [11]. On the basis of this research, the ambient vibration measurements were conducted to investigate the deck-stay interaction. It was suggested that the nonlinear coupling is not consistent with the measurement data. In contrast, the linear coupling is recognized as the critical excitation source of the coupled modes [16].

In parallel to the previous work [11, 16], the authors of the present paper also studied the deck-stay interaction of cable-stayed bridges based on the analytical and numerical methods as well as the long-term comprehensive full-scale measurements [17]. The measurement data indicated that the deck oscillations of small to moderate amplitudes are coupled with the large-amplitude stay cable vibrations due to the linear coupling between these two components. An analytical model of the single cable with spring-mass oscillator was presented to explain such mechanism attributed to the frequency loci veering and mode localization. Furthermore, the “pure” deck modes, “pure” cable modes and coupled modes are successfully captured by the proposed model. These phenomena are verified by the numerical simulations of the OECS and MECS models of a full cable-stayed bridge. The concepts of the indices for quantitatively assessing the degree of coupling among the structural components were also appeared in this research.

It is important to investigate the deck-stay interaction with the appropriate initial shape of a cable-stayed bridge. This is because such initial shape not only reasonably provides the geometric configuration as well as the prestress distribution of the bridge under the weight of the deck-tower system and the pretension forces in the stay cables, but also definitely ensures the satisfaction of the relations for the equilibrium conditions, boundary conditions

and architectural design requirements [18-21]. The computational procedures for the initial shape analyses of the OECS and MECS models were presented for this reason [22, 23]. However, few researchers have studied the deck-stay interaction with the initial shape effect.

The objective of this study is to fully understand the mechanism of the deck-stay interaction with the appropriate initial shapes of cable-stayed bridges. Based on the smooth and convergent bridge shapes obtained by the initial shape analysis [22, 23], the OECS and MECS models of the Kao Ping Hsi Bridge in southern Taiwan are developed to verify the applicability of the analytical model and numerical formulation from the field observations [17]. For this purpose, the modal analyses of the two finite element models are conducted to calculate the natural frequency and normalized mode shape of the individual modes of the bridge. The modal coupling assessment is also performed to obtain the generalized mass ratios among the structural components for each mode of the bridge [24]. To further investigate the deck-stay interaction characteristics of cable-stayed bridges under earthquake excitations, the dynamic displacements and internal forces of the two finite element models are calculated based on the seismic analyses. These results can be used to provide a variety of viewpoints to illustrate the mechanism of the deck-stay interaction with the appropriate initial shapes of cable-stayed bridges.

2. Finite element formulation

On the basis of the finite element concepts, a cable-stayed bridge can be considered as an assembly of a finite number of cable elements for the stay cables and beam-column elements for both the decks and towers. Several assumptions are adopted in this study: the material is homogeneous and isotropic; the stress-strain relationship of the material remains within the linear elastic range during the whole nonlinear response; the external forces are displacement independent; large displacements and large rotations are allowed, but strains are small; each stay cable is fixed to both the deck and tower at their joints of attachment. Based on the system equations with the consideration of geometric nonlinearities, the initial shape analysis, modal analysis, modal coupling assessment and seismic analysis of cable-stayed bridges are conducted in this study.

2.1. Geometric nonlinearities

To reasonably simulate cable-stayed bridges, three types of geometric nonlinearities: the cable sag, beam-column and large displacement effects, are considered in this study.

A stay cable will sag into a catenary shape due to its weight and tensile force. Such cable sag effect has to be taken into consideration when the stay cable is represented by a single straight cable element. A stay cable with tensile stiffness is assumed to be perfectly elastic. The compressive, shear and bending stiffnesses of the stay cable are negligible. The cable sag nonlinearity can be simulated based on the equivalent modulus of elasticity of the stay cable [25]

$$E_{eq} = \frac{E_c}{1 + \frac{(wl_c)^2 A_c E_c}{12T^3}}, \tag{1}$$

where E_c, A_c and l_c are the effective modulus of elasticity, the cross-sectional area and the horizontal projected length of the stay cable, respectively; w is the weight of the stay cable per unit length; T is the tension in the stay cable. The stiffness matrix of a cable element in Figure 1 can be expressed as

$$KE_{jk} = \begin{cases} \left[\frac{E_{eq}A_c}{L_c}\right], & u_1 > 0 \\ [0], & u_1 \le 0 \end{cases}, \tag{2}$$

where u_1 is the element coordinate for the relative axial deformation; L_c is the chord length of the stay cable.

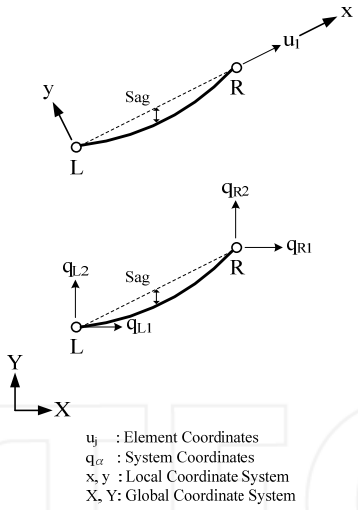

Figure 1. Cable element for simulating the stiffness of each stay cable.

High pretension forces in the stay cables can result in large compressive forces in the deck-tower system of a cable-stayed bridge. For this reason, the beam-column effect between such compressive forces and bending moments has to be considered when beam-column elements are used to simulate both the decks and towers. For a beam-column element based on the Euler-Bernoulli beam theory in Figure 2, shear strains of the element are neglected. u_1, u_2 and u_3 are the element coordinates for the left end rotation, the right end rotation and the relative axial deformation, respectively. The stiffness matrix of the beam-column element can be written as

$$KE_{jk} = \frac{E_b I_b}{L_b}\begin{bmatrix} C_s & C_t & 0 \\ C_t & C_s & 0 \\ 0 & 0 & R_t A_b / I_b \end{bmatrix}, \tag{3}$$

where E_b, A_b, I_b and L_b are the modulus of elasticity, the cross-sectional area, the moment of inertia and the length of the beam-column element, respectively; C_s, C_t and R_t are the stability functions representing the interaction between the axial and bending stiffnesses of the beam-column element [26].

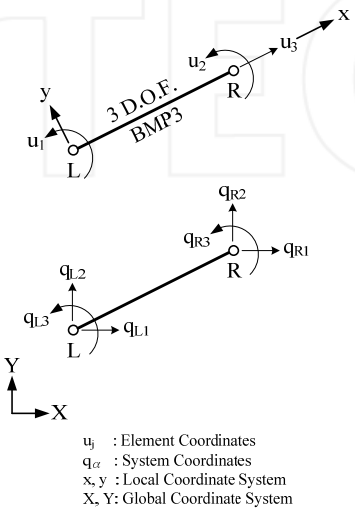

Figure 2. Beam-column element for simulating the stiffness of each deck and tower.

In general, large displacements occur in the deck-tower system due to the large span and less weight of a cable-stayed bridge. Such effect has to be taken into consideration when the equilibrium equations are derived from the deformed position. Under these conditions, the element coordinate u_j can be expressed as a nonlinear function of the system coordinate q_α in both Figure 1 and Figure 2, i.e., $u_j = u_j(q_\alpha)$. By differentiating u_j with respect to q_α, the first-order and second-order coordinate transformation coefficients can be individually written as

$$a_{j\alpha} = \frac{\partial u_j}{\partial q_\alpha}, \tag{4}$$

$$a_{j\alpha,\beta} = \frac{\partial a_{j\alpha}}{\partial q_\beta} = \frac{\partial^2 u_j}{\partial q_\alpha \partial q_\beta}. \tag{5}$$

$a_{j\alpha}$ and $a_{j\alpha,\beta}$ for the stiffness matrices of the cable and beam-column elements can be found in [18], which are provided to develop the tangent system stiffness matrix in Chapter 2.2.

In addition to the element stiffness matrices, the element mass matrices are introduced to fully understand the essential properties of a cable-stayed bridge. Based on the consistent mass model, the mass distribution of each stay cable and that of each deck and tower can be simulated by a cable element and a beam-column element, respectively. The mass matrix of the former with four element coordinates $u_j \ (j=1-4)$ in Figure 3 and that of the latter with six element coordinates $u_j \ (j=1-6)$ in Figure 4 can be individually expressed as

$$ME_{jk} = \frac{\rho_c A_c L_c}{6}\begin{bmatrix} 2 & 0 & 1 & 0 \\ 0 & 2 & 0 & 1 \\ 1 & 0 & 2 & 0 \\ 0 & 1 & 0 & 2 \end{bmatrix}, \tag{6}$$

$$ME_{jk} = \frac{\rho_b A_b L_b}{420}\begin{bmatrix} 140 & 0 & 0 & 70 & 0 & 0 \\ 0 & 156 & 22L_b & 0 & 54 & -13L_b \\ 0 & 22L_b & 4L_b^2 & 0 & 13L_b & -3L_b^2 \\ 70 & 0 & 0 & 140 & 0 & 0 \\ 0 & 54 & 13L_b & 0 & 156 & -22L_b \\ 0 & -13L_b & -3L_b^2 & 0 & -22L_b & 4L_b^2 \end{bmatrix}, \tag{7}$$

where ρ_c and ρ_b are the mass densities of the cable and beam-column elements, respectively. The coordinate transformation coefficient $a_{j\alpha}$ connected between u_j and q_α for the mass matrices of the cable and beam-column elements can be found in [20].

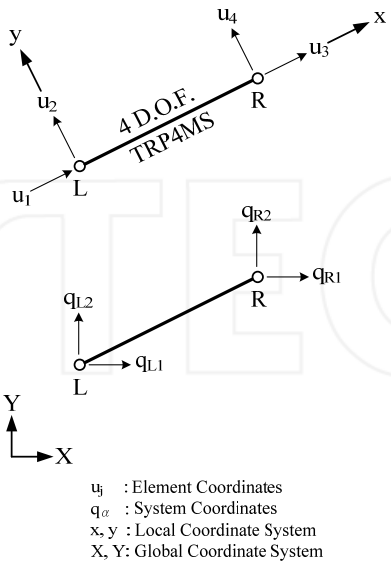

Figure 3. Cable element for simulating the mass of each stay cable.

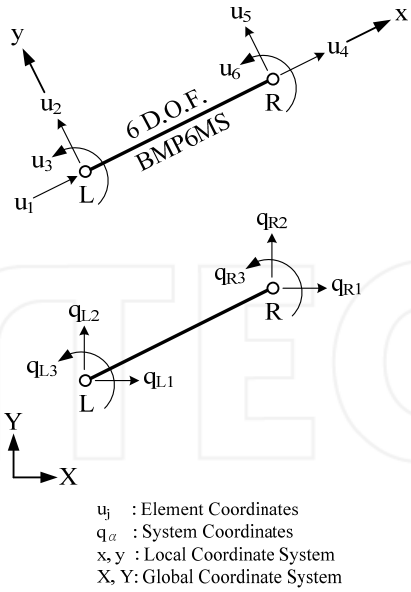

Figure 4. Beam-column element for simulating the mass of each deck and tower.

2.2. System equations

The system equations in generalized coordinates of a nonlinear finite element model of a cable-stayed bridge can be derived from the Lagrange's virtual work principle

$$M_{\alpha\beta}\ddot{q}_\beta + D_{\alpha\beta}\dot{q}_\beta + \sum_{EL} S_j a_{j\alpha} = P_\alpha, \quad \alpha = 1,2,3,\cdots,N, \tag{8}$$

$$M_{\alpha\beta} = \sum_{EL} ME_{jk} a'_{j\alpha} a'_{k\beta}, \tag{9}$$

$$S_j = KE_{jk} u_k + S_j^0, \tag{10}$$

$$P_\alpha = \vec{K}^j \cdot \vec{b}_\alpha^j \quad , \tag{11}$$

$$\vec{b}_\alpha^j = \frac{\partial \vec{W}^j}{\partial q_\alpha}, \tag{12}$$

$$\dot{q}_\alpha = \frac{dq_\alpha}{dt} \quad , \tag{13}$$

$$\ddot{q}_\alpha = \frac{d^2 q_\alpha}{dt^2} \quad , \tag{14}$$

where $M_{\alpha\beta}$ and $D_{\alpha\beta}$ are the system mass and damping matrices, respectively, which both are assumed to be constant; S_j is the element force vector; P_α is the external force vector; S_j^0 is the initial element force vector; $\bar{K}^j$ is the external nodal force vector; $\bar{b}_\alpha^j$ is the basis vector; $\bar{W}^j$ is the displacement vector corresponding to $\bar{K}^j$; $\dot{q}_\alpha$ and $\ddot{q}_\alpha$ are the system velocity and acceleration vectors, respectively; t is the time; N is the number of degrees of freedom; the subscripts α and β denote the numbers of the system coordinates; the subscripts j and k represent the numbers of the element coordinates; the superscript j denotes the nodal number; $\sum_{EL}$ represents the summation over all elements.

Under consideration of three types of geometric nonlinearities mentioned in Chapter 2.1, KE_{jk} of a cable element and that of a beam-column element can be individually obtained from Eq. (2) and Eq. (3). The former and the latter are due to the cable sag effect and the beam-column effect, respectively. Similarly, ME_{jk} of the cable element and that of the beam-column element can be individually obtained from Eq. (6) and Eq. (7). u_j, $a_{j\alpha}$ and $\bar{b}_\alpha^j$ are nonlinear functions of q_α when the large displacement effect occurs. $\bar{K}^j$ can be written as a function of q_α if they are displacement dependent forces. $M_{\alpha\beta}$ and $D_{\alpha\beta}$ are both assumed to be constant, because only nonlinearities in stiffness are considered in this system.

Eq. (8) is a set of simultaneous second-order nonlinear ordinary differential equations. In order to incrementally solve these equations, the linearized system equations in a small time (or force) interval are derived based on the first-order Taylor series expansion of Eq. (8)

$$M_{\alpha\beta}\Delta\ddot{q}_\beta^n + D_{\alpha\beta}\Delta\dot{q}_\beta^n + {}^2K_{\alpha\beta}^n\Delta q_\beta^n = {}_uP_\alpha^n + \Delta P_\alpha^n, \quad t^n \le t \le t^n + \Delta t^n, \tag{15}$$

$${}^2K_{\alpha\beta}^n = \sum_{EL} KE_{jk}^n a_{j\alpha}^n a_{k\beta}^n + \sum_{EL} S_j^n a_{j\alpha,\beta}^n - {}^n\bar{K}^j \cdot {}^n\bar{b}_{\alpha,\beta}^j - {}^n\bar{K}_\beta^j \cdot {}^n\bar{b}_\alpha^j, \tag{16}$$

$$\bar{b}_{\alpha,\beta}^j = \frac{\partial \bar{b}_\alpha^j}{\partial q_\beta}, \tag{17}$$

$$\bar{K}_\alpha^j = \frac{\partial \bar{K}^j}{\partial q_\alpha} \tag{18}$$

$${}_uP_\alpha^n = P_\alpha^n - M_{\alpha\beta}\ddot{q}_\beta^n - D_{\alpha\beta}\dot{q}_\beta^n - \sum_{EL} S_j^n a_{j\alpha}^n, \tag{19}$$

$$\Delta P_\alpha^n = P_\alpha^{n+1} - P_\alpha^n, \tag{20}$$

$$\Delta q_\alpha^n = q_\alpha^{n+1} - q_\alpha^n, \tag{21}$$

$$\Delta \dot{q}_\alpha^n = \dot{q}_\alpha^{n+1} - \dot{q}_\alpha^n, \tag{22}$$

$$\Delta \ddot{q}_\alpha^n = \ddot{q}_\alpha^{n+1} - \ddot{q}_\alpha^n, \tag{23}$$

$$\Delta t^n = t^{n+1} - t^n, \tag{24}$$

where ${}^2K_{\alpha\beta}^n$ is the tangent system stiffness matrix; ${}_uP_\alpha^n$ is the unbalanced force vector; ΔP_α^n is the increment of the external force vector; Δq_α^n, $\Delta \dot{q}_\alpha^n$ and $\Delta \ddot{q}_\alpha^n$ are the increments of the system coordinate, velocity and acceleration vectors, respectively; Δt^n is the time increment; the superscript n and $n+1$ denote the numbers of the time (or force) steps; the superscript 2 represents the second-order iteration matrix.

${}^2K_{\alpha\beta}^n$ in Eq. (16) consists of four terms. The first term is the elastic stiffness matrix, while the second and third terms are the geometric stiffness matrices induced by large displacements. Furthermore, the fourth term is the geometric stiffness matrix induced by displacement dependent forces, which is neglected in this study.

Eq. (15) is a set of simultaneous second-order linear ordinary differential equations in a small time interval, which can be solved by the direct integration method [20].

2.3. Initial shape analysis

The initial shape of a cable-stayed bridge provides the geometric configuration as well as the prestress distribution of such bridge under the weight of the deck-tower system and the pretension forces in the stay cables. The relations for the equilibrium conditions, boundary conditions and architectural design requirements should be satisfied. Under consideration of three types of geometric nonlinearities, i.e., the cable sag, beam-column and large displacement effects, the initial shape analyses of an OECS model and a MECS model are presented in this study.

For the initial shape analysis of the OECS model, the weight of the deck-tower system is considered, whereas the weight of the stay cables is neglected. The shape finding computation is performed using a two-loop iteration method: an equilibrium iteration and a shape iteration [18-23]. It can be started with an estimated initial element force (pretension force) in the stay cables. Based on the reference configuration (architectural design form) with no deflection and zero prestress in the deck-tower system, the equilibrium configuration of the whole bridge under the weight of the deck-tower system can be first determined by incrementally solving the linearized system equations

$$ {}^2K_{\alpha\beta}^n \Delta q_\beta^n = {}_uP_\alpha^n + \Delta P_\alpha^n, \quad P_\alpha^n \le P_\alpha \le P_\alpha^{n+1}, \tag{25} $$

$$ {}_uP_\alpha^n = P_\alpha^n - \sum_{EL} S_j^n a_{j\alpha}^n, \tag{26} $$

which are individually derived from Eq. (15) and Eq. (19) with negligible inertial and damping effects due to the static case. On the basis of Eq. (25) and Eq. (26), the equilibrium iteration is performed using the Newton-Raphson method [18-23].

After the above equilibrium iteration, the bridge configuration satisfies the equilibrium and boundary conditions, however, the architectural design requirements are, in general, not fulfilled. This is because large displacements and variable bending moments occur in the deck-tower system due to the large bridge span. Under these conditions, the shape iteration

is conducted to reduce the displacements and to smooth the bending moments, and the appropriate initial shape can therefore be obtained.

A number of control points are selected for insuring that both the deck and tower displacements satisfy the architectural design requirements in the shape iteration

$$\left|\frac{q_\alpha}{L_r}\right| \le \varepsilon_r, \tag{27}$$

where q_α is the displacement in a certain direction of the control point; L_r is the reference length; ε_r is the convergence tolerance. For checking the deck displacement, each control point is the node intersected by the deck and the stay cable. q_α and L_r individually denote the vertical displacement of the control point and the main span length. Similarly, each node intersected by the tower and the stay cable, or located on the top of the tower is chosen as the control point for checking the tower displacement. q_α and L_r represent the horizontal displacement of the control point and the tower height, respectively.

If Eq. (27) is not achieved, the element axial forces calculated in the previous equilibrium iteration will be taken as the initial element forces in the new equilibrium iteration, and the corresponding equilibrium configuration of the whole bridge under the weight of the deck-tower system will be determined again. The shape iteration will then be repeated until Eq. (27) is reached. Under these conditions, the convergent configuration can be regarded as the initial shape of the OECS model.

The initial shape analysis of the MECS model is also performed to reasonably simulate the bridge configuration. Based on the initial shape of the OECS model obtained previously, the both end coordinates and pretension force in each single stay cable can be used for the shape finding computation of the corresponding stay cable discretized into multiple elements using the catenary function method [22, 23]. Incorporating the interior nodal coordinates and pretension forces in each discrete stay cable into the bridge model, and then conducting the two-loop iteration method again, the convergent configuration can be regarded as the initial shape of the MECS model.

2.4. Modal analysis

Under the assumption that the system vibrates with a small amplitude around a certain nonlinear static state, in which the variation in such state induced by the vibration is negligible, the modal analysis of a cable-stayed bridge can be conducted based on the linearized system equation

$$M^A_{\alpha\beta}\ddot{q}_\beta + {}^2K^A_{\alpha\beta}q_\beta = 0, \tag{28}$$

where $M^A_{\alpha\beta}$ and ${}^2K^A_{\alpha\beta}$ are the system mass and tangent system stiffness matrices with respect to the nonlinear static state q^A_α, respectively. The initial shape obtained in Chapter 2.3 can be regarded as q^A_α. Eq. (28) is derived from Eq. (15) with negligible damping and

force effects. On the basis of Eq. (28) representing the free vibration of the undamped system, the natural frequency f_n and the normalized mode shape $\bar{Y}_n$ of the n th mode can be calculated by the subspace iteration method [20].

2.5. Modal coupling assessment

According to the results of both the initial shape analysis (Chapter 2.3) and modal analysis (Chapter 2.4) with the consideration of geometric nonlinearities (Chapter 2.1) in the system equations (Chapter 2.2), three indices for quantitatively assessing the degree of coupling among the stay cables, decks and towers of a cable-stayed bridge in each mode are presented [24] as

$$\bar{M}_n^s = \frac{\left(\bar{Y}_n^s\right)^T M^s \bar{Y}_n^s}{\left(\bar{Y}_n^s\right)^T M^s \bar{Y}_n^s + \left(\bar{Y}_n^d\right)^T M^d \bar{Y}_n^d + \left(\bar{Y}_n^t\right)^T M^t \bar{Y}_n^t}, \tag{29}$$

$$\bar{M}_n^d = \frac{\left(\bar{Y}_n^d\right)^T M^d \bar{Y}_n^d}{\left(\bar{Y}_n^s\right)^T M^s \bar{Y}_n^s + \left(\bar{Y}_n^d\right)^T M^d \bar{Y}_n^d + \left(\bar{Y}_n^t\right)^T M^t \bar{Y}_n^t}, \tag{30}$$

$$\bar{M}_n^t = \frac{\left(\bar{Y}_n^t\right)^T M^t \bar{Y}_n^t}{\left(\bar{Y}_n^s\right)^T M^s \bar{Y}_n^s + \left(\bar{Y}_n^d\right)^T M^d \bar{Y}_n^d + \left(\bar{Y}_n^t\right)^T M^t \bar{Y}_n^t}, \tag{31}$$

where $\bar{M}_n^j \ \left(j = s,d,t\right)$ are the generalized mass ratios of the n th mode; $M^j \ \left(j = s,d,t\right)$ are the submatrices of $M_{\alpha\beta}^A$; $\bar{Y}_n^j \ \left(j = s,d,t\right)$ are the subvectors of $\bar{Y}_n$ in the n th mode; the superscripts s, d and t denote the quantities of the stay cable, the deck and the tower, respectively. The sum of $\bar{M}_n^s$, $\bar{M}_n^d$ and $\bar{M}_n^t$ is 1 for the corresponding n.

2.6. Seismic analysis

According to the assumption that the system is under the uniform earthquake excitation, the seismic analysis of a cable-stayed bridge with respect to the initial shape obtained in Chapter 2.3 can be conducted based on the equivalent difference equations

$${}^*Q_\alpha^{n+1} = {}^*K_{\alpha\beta}^n \Delta q_\beta^n, \quad t^n \le t \le t^n + \Delta t^n, \tag{32}$$

$${}^*Q_\alpha^{n+1} = P_\alpha^{n+1} - M_{\alpha\beta}\, {}^*\ddot{q}_\beta^n - D_{\alpha\beta}\, {}^*\dot{q}_\beta^n - \sum_{EL} S_j^n a_{j\alpha}^n, \tag{33}$$

$${}^*K_{\alpha\beta}^n = I_1 M_{\alpha\beta} + I_2 D_{\alpha\beta} + {}^2K_{\alpha\beta}^n, \tag{34}$$

$$P_\alpha^n = -M_{\alpha\beta} I_\beta\, {}^g\ddot{q}^n, \tag{35}$$

$$ {}^{*}\dot{q}_{\alpha}^{n} = -I_4\dot{q}_{\alpha}^{n} - I_6\ddot{q}_{\alpha}^{n}, \tag{36} $$

$$ {}^{*}\ddot{q}_{\alpha}^{n} = -I_3\dot{q}_{\alpha}^{n} - I_5\ddot{q}_{\alpha}^{n}, \tag{37} $$

$$ q_{\alpha}^{n+1} = q_{\alpha}^{n} + \Delta q_{\alpha}^{n}, \tag{38} $$

$$ \dot{q}_{\alpha}^{n+1} = {}^{*}\dot{q}_{\alpha}^{n} + I_2\Delta q_{\alpha}^{n}, \tag{39} $$

$$ \ddot{q}_{\alpha}^{n+1} = {}^{*}\ddot{q}_{\alpha}^{n} + I_1\Delta q_{\alpha}^{n}, \tag{40} $$

$$ I_1 = \frac{1}{\beta_1\left(\Delta t^{n}\right)^{2}}, \tag{41} $$

$$ I_2 = \frac{\gamma_1}{\beta_1\Delta t^{n}}, \tag{42} $$

$$ I_3 = \frac{1}{\beta_1\Delta t^{n}}, \tag{43} $$

$$ I_4 = \frac{1}{2\beta_1} - 1, \tag{44} $$

$$ I_5 = \frac{\gamma_1}{\beta_1} - 1, \tag{45} $$

$$ I_6 = \left(\frac{\gamma_1}{2\beta_1} - 1\right)\Delta t^{n}, \tag{46} $$

where these equations are derived from Eq. (15) and Eq. (19) using the Newmark method [27]; ${}^{*}Q_{\alpha}^{n+1}$ is the effective force vector; ${}^{*}K_{\alpha\beta}^{n}$ is the effective system stiffness matrix; ${}^{g}\ddot{q}^{n}$ is the earthquake-induced ground acceleration; I_{β} is the column vector in which each element is either zero or unity depending on the direction of ${}^{g}\ddot{q}^{n}$; β_1 and γ_1 are the parameters defining the variation of acceleration over a time increment and determining the stability and accuracy characteristics of the Newmark method; ${}^{*}\dot{q}_{\alpha}^{n}$, ${}^{*}\ddot{q}_{\alpha}^{n}$ and I_j $\left(j = 1-6\right)$ are the coefficients of the seismic analysis.

2. Finite element models

To understand the deck-stay interaction with the appropriate initial shapes of cable-stayed bridges, an OECS model and a MECS model of the full Kao Ping Hsi Bridge are developed, as shown in Figure 5(a) and 5(b), respectively. This bridge is an unsymmetrical single-deck cable-stayed bridge with a main span of 330 m and a side span of 184 m. The deck, which

consists of steel box girders in the main span and concrete box girders in the side span, is supported by a total of 28 stay cables (S1-S28), arranged in a central plane originated at the 184 m tall, inverted Y-shaped, concrete tower. A more detailed description of the Kao Ping Hsi Bridge can be found in [28].

Figure 5(a) and 5(b) illustrate the two-dimensional finite element models of the bridge. The OECS and MECS models both contain 48 beam-column elements that simulate the deck and tower. For the MECS model, each stay cable is discretized into 10 cable elements, whereas a single cable element is used to simulate each stay cable in the OECS model. This fact indicates that the OECS and MECS models individually include 28 and 280 cable elements. Figure 5(a) and 5(b) also show that 49 and 301 nodes are involved in the OECS and MECS models, respectively. A hinge, roller and fixed supports are used to model the boundary conditions of the left and right ends of the deck and the tower, respectively, and a rigid joint is employed to simulate the deck-tower connection. On the basis of the OECS and MECS models, the initial shape analysis, modal analysis, modal coupling assessment and seismic analysis of the Kao Ping Hsi Bridge are conducted in this study.

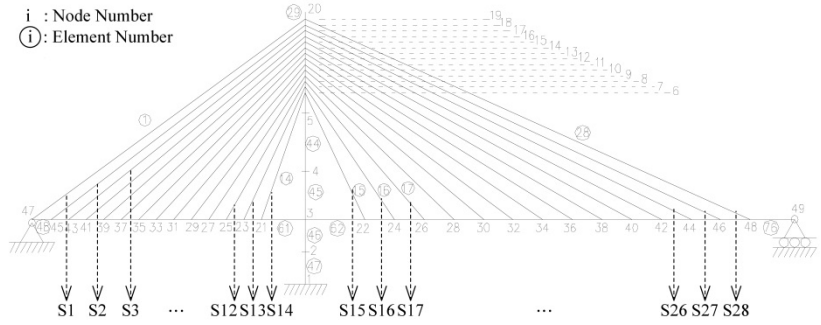

(a) OECS model

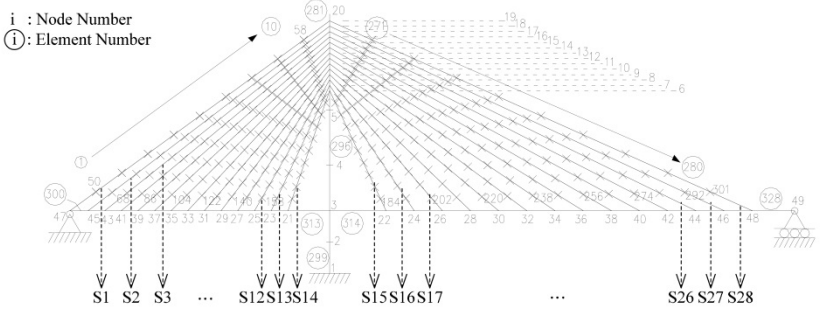

(b) MECS model

Figure 5. Finite element models of the Kao Ping Hsi Bridge.

4. Numerical results

Based on the OECS and MECS models of the Kao Ping Hsi Bridge developed in Chapter 3, the initial shape analysis, modal analysis, modal coupling assessment and seismic analysis are conducted using the finite element formulation presented in Chapter 2. The numerical results can be used to fully understand the mechanism of the deck-stay interaction with the appropriate initial shapes of cable-stayed bridges.

4.1. Initial shape analysis

Based on the finite element procedures presented in Chapter 2.3, the initial shape analyses of the OECS and MECS models are conducted to reasonably provide the geometric configuration of the Kao Ping Hsi Bridge. In both Figure 5(a) and 5(b), nodes 37, 38, 40, 45 and 46 are selected as the control points for checking the deck displacement in the vertical direction, while node 19 is chosen as the control point for checking the tower displacement in the horizontal direction. The convergence tolerance ε_r is set to 10^{-4} in this study.

Figure 6(a) shows the initial shape of the OECS model of the Kao Ping Hsi Bridge (solid line), indicating that the maximum vertical and horizontal displacements measured from the reference configuration (short dashed line) are 0.038 m at node 36 in the main span of the deck and -0.021 m at node 8 in the tower, respectively. The shape of each stay cable represented by a single cable element is straight as expected. Figure 6(a) also illustrates that the overall displacement obtained by the two-loop iteration method, i.e., the equilibrium and shape iterations, is comparatively smaller than that only from the equilibrium iteration (long dashed line). Consequently, the initial shape based on the two-loop iteration method appears to be able to appropriately describe the geometric configurations of cable-stayed bridges.

Figure 6(b) shows the initial shape of the MECS model of the Kao Ping Hsi Bridge (solid line), indicating that the maximum vertical and horizontal displacements measured from the reference configuration (short dashed line) are 0.068 m at node 34 in the main span of the deck and -0.049 m at node 8 in the tower, respectively. The sagged shape occurs in the stay cables due to the fact that each stay cable is simulated by multiple cable elements.

4.2. Modal analysis and modal coupling assessment

According to the results of the initial shape analysis presented in Chapter 4.1, the modal analyses of the OECS and MECS models using the finite element computations developed in Chapter 2.4 are conducted to calculate the natural frequency and normalized mode shape of the individual modes of the Kao Ping Hsi Bridge. The modal coupling assessment based on the proposed formulas in Chapter 2.5 is also performed to obtain the generalized mass ratios among the structural components for each mode of such bridge. These results can be used to provide a variety of viewpoints to illustrate the mechanism of the deck-stay interaction with the appropriate initial shapes of cable-stayed bridges.

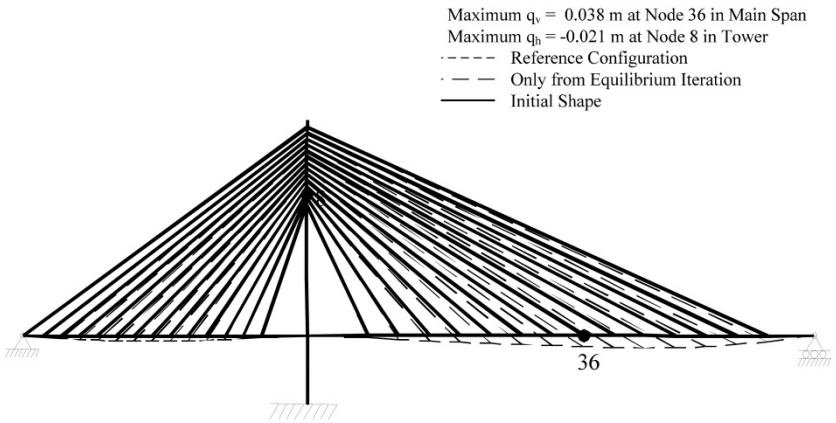

(a) OECS model

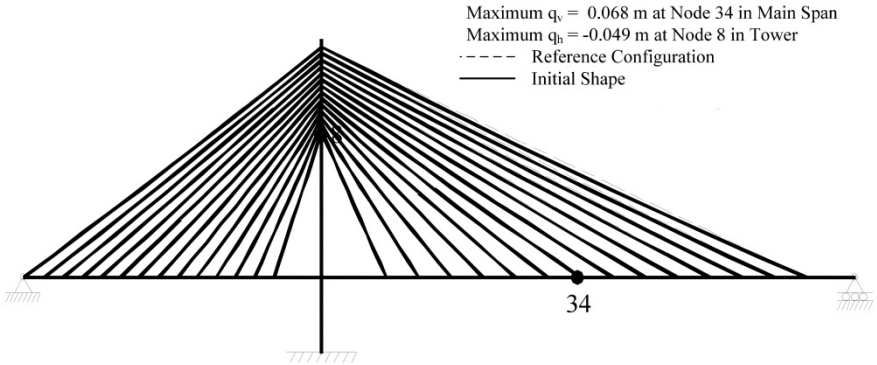

(b) MECS model

Figure 6. Initial shapes of the Kao Ping Hsi Bridge.

Table 1 summarizes the modal properties of the Kao Ping Hsi Bridge based on the OECS model (modes 1 to 3) and the MECS model (modes 1 to 24). In this table, f_n and $\overline{Y}_n$ represent the natural frequency and the normalized mode shape of the nth mode, respectively. As expected, the MECS model reveals the global, local and coupled modes, whereas the OECS model only yields the global modes. The modal properties of modes 1 and 2 in the OECS model are individually similar to those of modes 1 and 12 in the MECS model, because these modes represent the global modes. While mode 3 in the OECS model is identified as the global mode, mode 19 in the MECS model is the coupled mode. The other coupled mode can also be observed in mode 18 in the MECS model. These results suggest that the interaction between the deck-tower system and stay cables can be captured by the MECS model, but not by the OECS model. Also due to the limitations of the OECS model, modes 2 to 11, modes 13 to 17 and modes 20 to 24, which represent the local modes of the stay cables, are successfully captured by the MECS model, but not by the OECS model.

OECS				MECS			
n	f_n (Hz)	$\bar{Y}_n$	Type	n	f_n (Hz)	$\bar{Y}_n$	Type
1	0.2877	1st DT	G	1	0.3053	1st DT	G
				2	0.3382	1st S28	L
				3	0.3852	1st S27	L
				4	0.4274	1st S26	L
				5	0.4554	1st S1	L
				6	0.4653	1st S25	L
				7	0.4899	1st S24	L
				8	0.5067	1st S23	L
				9	0.5269	1st S22	L
				10	0.5378	1st S2	L
				11	0.5471	1st S21	L
2	0.5455	2nd DT	G	12	0.5686	2nd DT	G
				13	0.5944	1st S3	L
				14	0.6040	1st S20	L
				15	0.6333	1st S4	L
				16	0.6346	2nd S28	L
				17	0.6835	1st S5	L
				18	0.6850	3rd DT 1st S19	C
3	0.6854	3rd DT	G	19	0.7171	3rd DT 1st S19	C
				20	0.7269	1st S6	L
				21	0.7500	2nd S27	L
				22	0.7590	1st S7	L
				23	0.8008	1st S8	L
				24	0.8184	1st S18	L

DT: Deck-tower system
S: Stay cable
G: Global mode
L: Local mode
C: Coupled mode

Table 1. Comparisons between corresponding modal properties of the OECS and MECS models of the Kao Ping Hsi Bridge.

Figure 7 shows the relationship between the natural frequency and the mode number for the first 24 modes of the MECS model of the Kao Ping Hsi Bridge. For reference, the fundamental frequency of stay S19 (0.6908 Hz) is also included. This frequency is calculated based on the assumption that stay S19 is clamped at both ends [29].

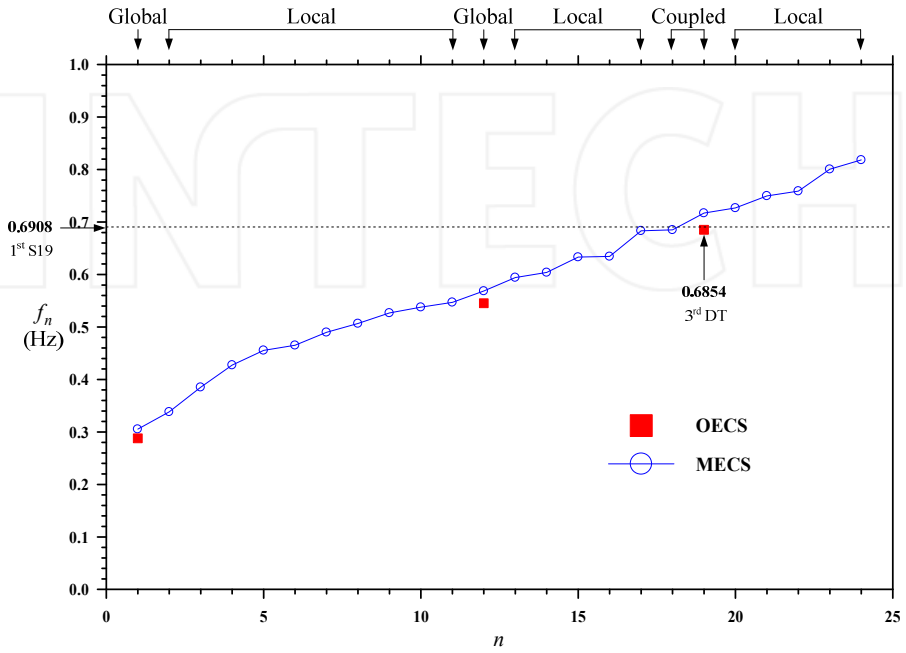

Figure 7. Relationships between natural frequencies and mode numbers of the MECS model of the Kao Ping Hsi Bridge.

Figure 8(a) and 8(b) illustrate the normalized mode shapes of the individual modes of the OECS model (modes 1 to 3) and the MECS model (modes 1 to 24) of the Kao Ping Hsi Bridge, respectively. Each normalized mode shape (solid line) is measured from the initial shape (dashed line) obtained in Chapter 4.1.

To quantitatively assess the degree of coupling for each mode, Figure 9 depicts the variations in the generalized mass ratios with respect to the mode number for the first 24 modes of the MECS model of the Kao Ping Hsi Bridge. In this figure, $\bar{M}_n^s$, $\bar{M}_n^d$ and $\bar{M}_n^t$ represent the generalized mass ratios of the stay cable, the deck and the tower of the n th mode, respectively. The sum of $\bar{M}_n^s$, $\bar{M}_n^d$ and $\bar{M}_n^t$ is 1 for the corresponding n $(n=1-24)$. It is evident that $\bar{M}_n^t$ $(n=1-24)$ approaches 0 for the first 24 modes due to the high rigidity of the concrete tower, resulting in the insignificant tower deformations in the lower modes sensitive to the ambient excitations, as can also be seen in Figure 8(b). These results are in agreement with the literature [2].

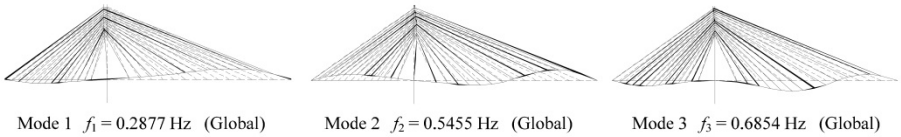

(a) OECS model

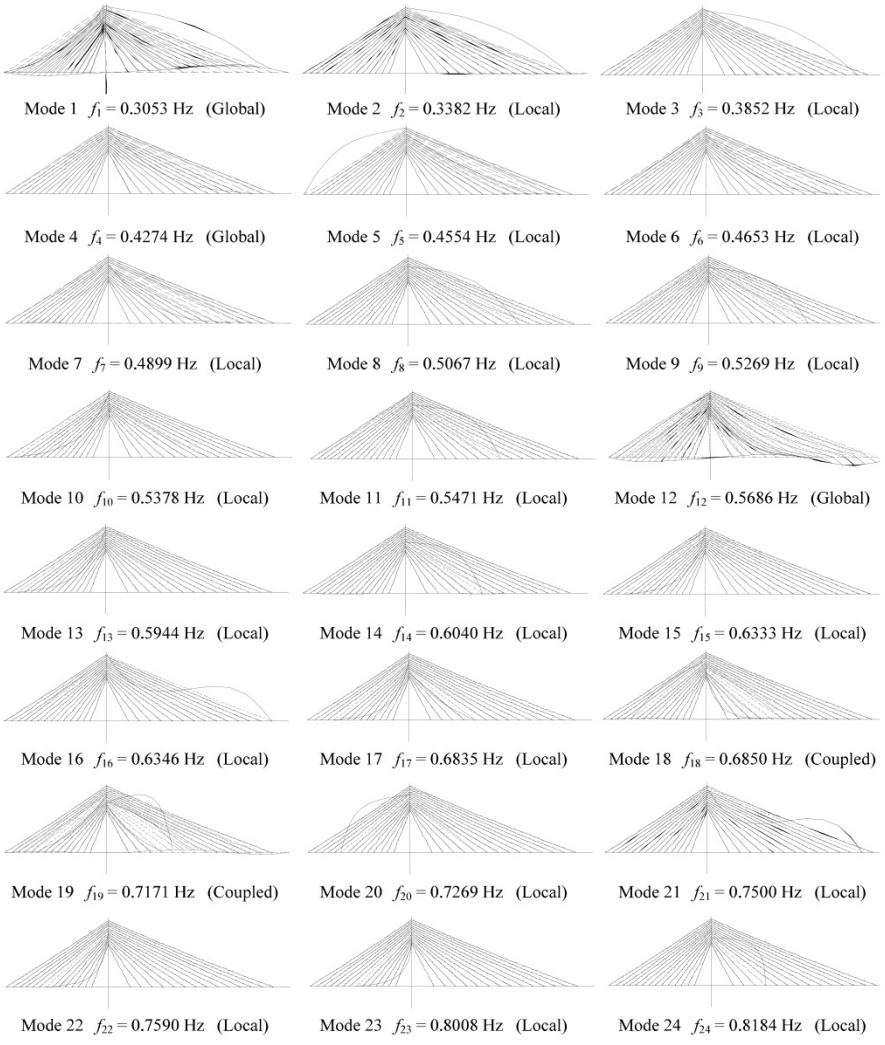

(b) MECS model

Figure 8. Normalized mode shapes of the Kao Ping Hsi Bridge.

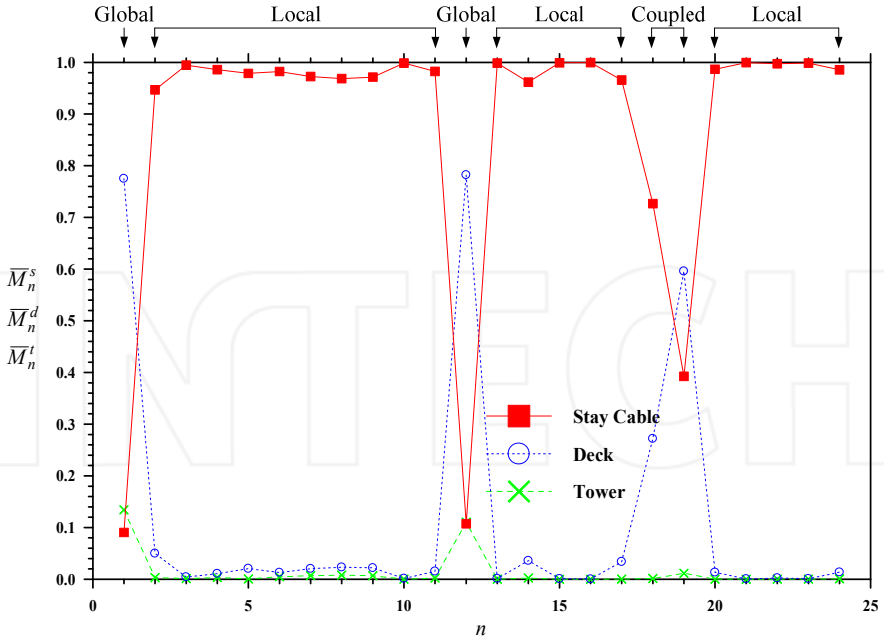

Figure 9. Variations in generalized mass ratios with respect to mode numbers of the MECS model of the Kao Ping Hsi Bridge.

It can be seen in Table 1, Figure 7, Figure 8(a) and 8(b) that for the global modes, f_n and $\overline{Y}_n$ $(n=1,2)$ in the OECS model are individually similar to f_n and $\overline{Y}_n$ $(n=1,12)$ in the MECS model. It is consistent with the results in Figure 9 that for modes 1 and 12 in the MECS model, the sum of $\overline{M}_n^d$ and $\overline{M}_n^t$ $(n=1,12)$ is close to 0.9, whereas $\overline{M}_n^s$ $(n=1,12)$ approaches 0.1. Consequently, these modes are primarily dominated by the deformations of the deck-tower system with the quasi-static motions of the stay cables. This type of response can be identified as the "pure" deck mode in the analytical model [17].

It also can be seen in Figure 9 that for modes 2 to 11, modes 13 to 17 and modes 20 to 24 in the MECS model, $\overline{M}_n^s$ $(n=2-11,13-17,20-24)$ is close to 1, whereas the sum of $\overline{M}_n^d$ and $\overline{M}_n^t$ $(n=2-11,13-17,20-24)$ approaches 0. It is consistent with the results in Table 1, Figure 7 and Figure 8(b) that $\overline{Y}_n$ $(n=2-11,13-17,20-24)$ in the MECS model is the local mode predominantly consisting of the stay cable motions with negligible deformations of the deck-tower system. This type of response can be recognized as the "pure" cable mode in the analytical model [17].

As shown in Table 1, Figure 7, Figure 8(a) and 8(b), the difference between f_{19} in the MECS model (0.7171 Hz) and f_3 in the OECS model (0.6854 Hz) is evident due to the fact that $\overline{Y}_{19}$ in the MECS model is the coupled mode, but $\overline{Y}_3$ in the OECS model is the global mode, i.e., the "pure" deck-tower mode. Similarly, f_{18} in the MECS model (0.6850 Hz) branches from the fundamental frequency of stay S19 clamped at both ends (0.6908 Hz). This is because

$\bar{Y}_{18}$ in the MECS model is the coupled mode, while the fundamental mode shape of stay S19 can be regarded as the "pure" stay cable mode. These observations are attributed to the frequency loci veering when the natural frequency of the "pure" deck-tower mode (0.6854 Hz) approaches that of the "pure" stay cable mode (0.6908 Hz). As illustrated in Figure 9, the sum of $\bar{M}_{19}^{d}$ and $\bar{M}_{19}^{t}$ is relatively higher than $\bar{M}_{19}^{s}$, whereas the sum of $\bar{M}_{18}^{d}$ and $\bar{M}_{18}^{t}$ is comparatively lower than $\bar{M}_{18}^{s}$. Consequently, $\bar{Y}_{18}$ and $\bar{Y}_{19}$ in the MECS model are the pair of coupled modes with the similar configurations, which have substantial contributions from both the deck-tower system and stay cables. These phenomena correspond to the mode localization. This type of response coincides with the coupled mode in the analytical model [17].

In summary, the coupled modes are attributed to the frequency loci veering and mode localization when the "pure" deck-tower frequency and the "pure" stay cable frequency approach one another, implying that the mode shapes of such coupled modes are simply different from those of the deck-tower system or stay cables alone. The distribution of the generalized mass ratios between the deck-tower system and stay cables are useful indices for quantitatively assessing the degree of coupling for each mode. These results are demonstrated to fully understand the mechanism of the deck-stay interaction with the appropriate initial shapes of cable-stayed bridges.

4.3. Seismic analysis

According to the results of the initial shape analysis presented in Chapter 4.1, the seismic analyses of the OECS and MECS models using the finite element computations developed in Chapter 2.6 are conducted to obtain the dynamic responses of the Kao Ping Hsi Bridge. Figure 10 shows the vertical component of the Chi-Chi earthquake accelerogram recorded in Mid-Taiwan on September 21, 1999 [30], which is selected as the earthquake-induced ground acceleration in this study. Under the excitation, the Newmark method $\left(\beta_1 = 1/4, \gamma_1 = 1/2\right)$ is used to calculate the displacement and internal force time histories of the system. The duration of the simulation is set to 30.0 s.

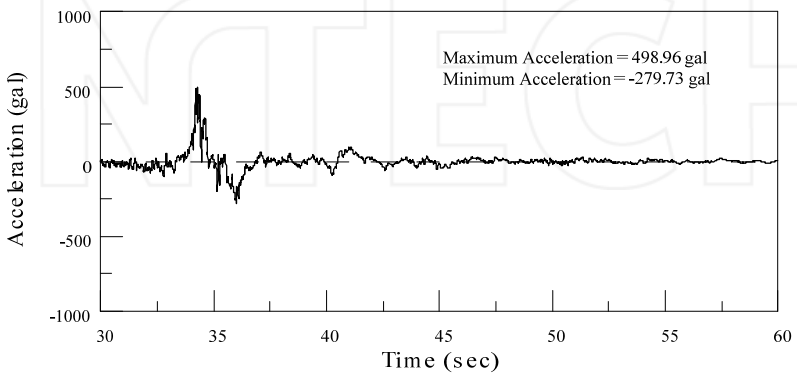

Figure 10. The Chi-Chi earthquake accelerogram.

Figure 11 shows the horizontal and vertical displacement time histories of nodes 295, 297 and 300 in stay S28 for the MECS model. The variations in the dynamic responses among the three nodes for each direction and those between the horizontal and vertical directions for each node are observed in this figure. Consequently, the dynamic displacements of the stay cables are successfully captured by the MECS model, but not by the OECS model. Figure 12 shows the vertical displacement time histories of nodes 35, 36 and 42 in the deck, the horizontal displacement time histories of nodes 8 and 20 in the tower, and the horizontal time history of node 49 in the right end of the deck, for both the OECS and MECS models. The dynamic response of each node in the OECS model coincides with that of the corresponding node in the MECS model. Consequently, the dynamic displacements of the deck-tower system are reasonably simulated by both the OECS and MECS models.

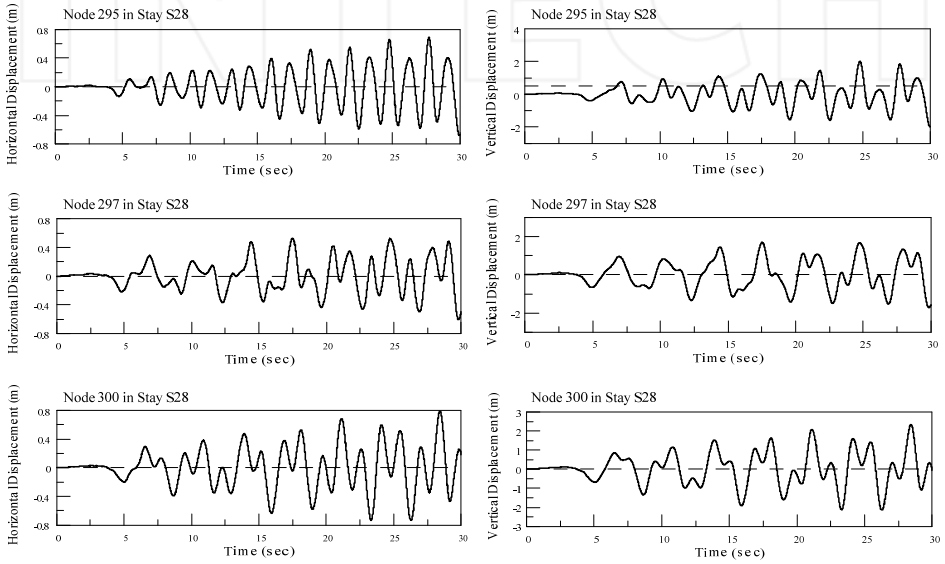

Figure 11. Displacement time histories of the stay cable of the Kao Ping Hsi Bridge.

The axial force, which is in the u_1 coordinate of the cable element in Figure 1, is the unique internal force of the stay cable. Figure 13 shows the internal force time history of element 28 in stay S28 for the OECS model and those of the corresponding elements 271, 275 and 280 in stay S28 for the MECS model. The variations in the dynamic responses among the three elements of the MECS model are negligible. In addition, the dynamic response of each element in the MECS model is in agreement with that of the corresponding element in the OECS model, which can be considered as the "nominal" dynamic axial force of the stay cable. Consequently, the dynamic internal forces of the stay cables are successfully captured by both the OECS and MECS models. The internal forces of the deck-tower system include the left moment, right moment and axial force, which are individually in the u_1, u_2 and u_3 coordinates of the beam-column element in Figure 2. Figure 14 shows the internal force time histories of element 69 (321) in the deck and those of element 40 (292) in the tower for the

OECS (MECS) model. The dynamic responses of each element in the OECS model coincide with those of the corresponding element in the MECS model. Consequently, the dynamic internal forces of the deck-tower system are reasonably simulated by both the OECS and MECS models.

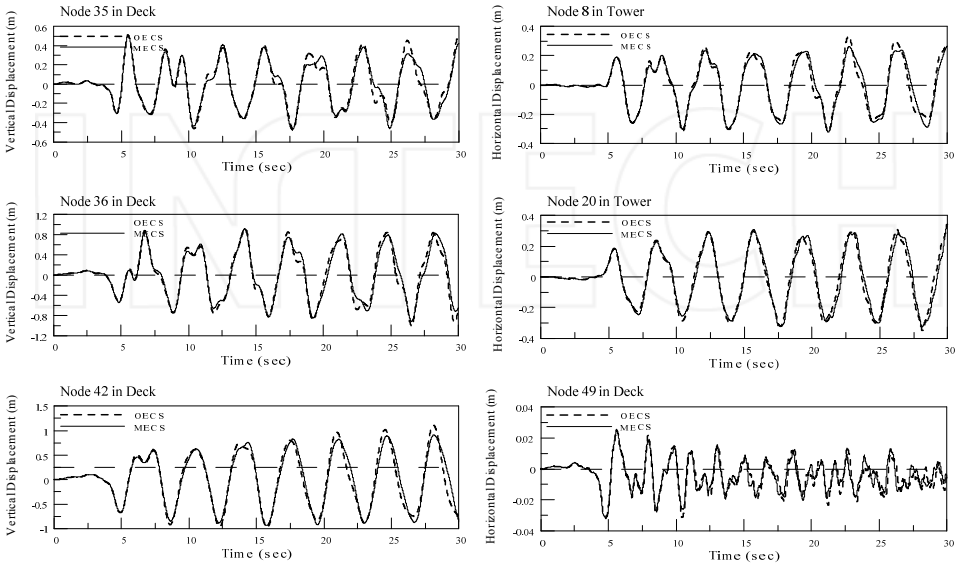

Figure 12. Displacement time histories of the deck-tower system of the Kao Ping Hsi Bridge.

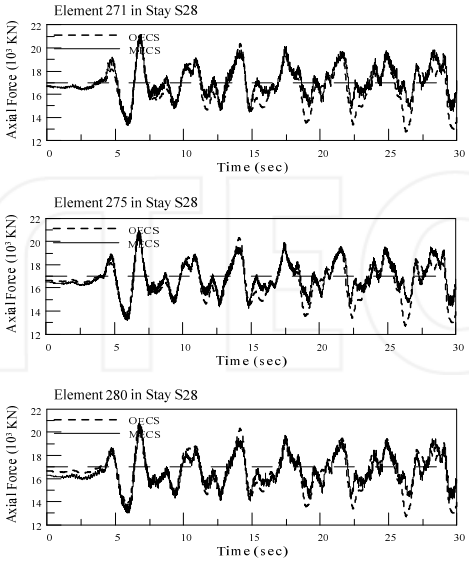

Figure 13. Internal force time histories of the stay cable of the Kao Ping Hsi Bridge.

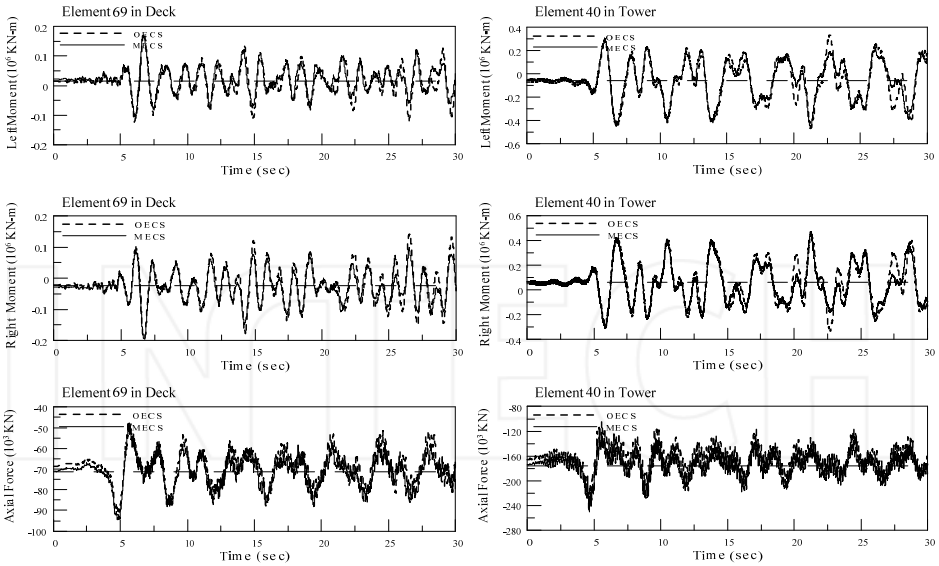

Figure 14. Internal force time histories of the deck-tower system of the Kao Ping Hsi Bridge.

In summary, the dynamic displacements of the stay cables are successfully captured by the MECS model, but not by the OECS model. Furthermore, the dynamic displacements of the deck-tower system as well as the dynamic internal forces of the stay cables and those of the deck-tower system are reasonably simulated by both the OECS and MECS models. These results are demonstrated to fully understand the deck-stay interaction characteristics of cable-stayed bridges under seismic excitations.

5. Conclusions

This study has provided a variety of viewpoints to illustrate the mechanism of the deck-stay interaction with the appropriate initial shapes of cable-stayed bridges. Based on the smooth and convergent bridge shapes obtained by the initial shape analysis, the OECS and MECS models of the Kao Ping Hsi Bridge are developed to verify the applicability of the analytical model and numerical formulation from the field observations in the authors' previous work. For this purpose, the modal analyses of the two finite element models are conducted to calculate the natural frequency and normalized mode shape of the individual modes of the bridge. The modal coupling assessment is also performed to obtain the generalized mass ratios among the structural components for each mode of the bridge. To further investigate the deck-stay interaction characteristics of cable-stayed bridges under earthquake excitations, the dynamic displacements and internal forces of the two finite element models are calculated based on the seismic analyses.

The findings indicate that the coupled modes are attributed to the frequency loci veering and mode localization when the "pure" deck-tower frequency and the "pure" stay cable

frequency approach one another, implying that the mode shapes of such coupled modes are simply different from those of the deck-tower system or stay cables alone. The distribution of the generalized mass ratios between the deck-tower system and stay cables are useful indices for quantitatively assessing the degree of coupling for each mode. To extend the two finite element models to be under the seismic excitation, it is evident that the dynamic displacements of the stay cables are successfully captured by the MECS model, but not by the OECS model. In addition, the dynamic displacements of the deck-tower system as well as the dynamic internal forces of the stay cables and those of the deck-tower system are reasonably simulated by both the OECS and MECS models. These results are demonstrated to fully understand the mechanism of the deck-stay interaction with the appropriate initial shapes of cable-stayed bridges.

Author details

Ming-Yi Liu and Pao-Hsii Wang
Department of Civil Engineering, Chung Yuan Christian University, Jhongli City, Taiwan

6. References

[1] Abdel-Ghaffar, A.M., and Khalifa, M.A. (1991). "Importance of cable vibration in dynamics of cable-stayed bridges." *Journal of Engineering Mechanics, ASCE*, 117(11), 2571-2589.

[2] Gimsing, N.J. (1997). "Cable supported bridges: Concept and design." Second Edition, John Wiley & Sons, Ltd, Chichester, UK.

[3] Fujino, Y., Warnitchai, P., and Pacheco, B.M. (1993). "An experimental and analytical study of autoparametric resonance in a 3DOF model of cable-stayed-beam." *Nonlinear Dynamics*, 4(2), 111-138.

[4] Warnitchai, P., Fujino, Y., Pacheco, B.M., and Agret, R. (1993). "An experimental study on active tendon control of cable-stayed bridges." *Earthquake Engineering and Structural Dynamics*, 22(2), 93-111.

[5] Warnitchai, P., Fujino, Y., and Susumpow, T. (1995). "A non-linear dynamic model for cables and its application to a cable-structure system." *Journal of Sound and Vibration*, 187(4), 695-712.

[6] Lilien, J.L., and Pinto da Costa, A. (1994). "Vibration amplitudes caused by parametric excitation of cable stayed structures." *Journal of Sound and Vibration*, 174(1), 69-90.

[7] Pinto da Costa, A., Martins, J.A.C., Branco, F., and Lilien, J.L. (1996). "Oscillations of bridge stay cables induced by periodic motions of deck and/or towers." *Journal of Engineering Mechanics, ASCE*, 122(7), 613-622.

[8] Gattulli, V., Morandini, M., and Paolone, A. (2002). "A parametric analytical model for non-linear dynamics in cable-stayed beam." *Earthquake Engineering and Structural Dynamics*, 31(6), 1281-1300.

[9] Gattulli, V., and Lepidi, M. (2003). "Nonlinear interactions in the planar dynamics of cable-stayed beam." *International Journal of Solids and Structures*, 40(18), 4729-4748.

[10] Gattulli, V., Lepidi, M., Macdonald, J.H.G., and Taylor, C.A. (2005). "One-to-two global-local interaction in a cable-stayed beam observed through analytical, finite element and experimental models." *International Journal of Non-Linear Mechanics*, 40(4), 571-588.

[11] Gattulli, V., and Lepidi, M. (2007). "Localization and veering in the dynamics of cable-stayed bridges." *Computers and Structures*, 85(21-22), 1661-1678.

[12] Tuladhar, R., Dilger, W.H., and Elbadry, M.M. (1995). "Influence of cable vibration on seismic response of cable-stayed bridges." *Canadian Journal of Civil Engineering*, 22(5), 1001-1020.

[13] Caetano, E., Cunha, A., and Taylor, C.A. (2000a). "Investigation of dynamic cable-deck interaction in a physical model of a cable-stayed bridge. Part I: modal analysis." *Earthquake Engineering and Structural Dynamics*, 29(4), 481-498.

[14] Caetano, E., Cunha, A., and Taylor, C.A. (2000b). "Investigation of dynamic cable-deck interaction in a physical model of a cable-stayed bridge. Part II: seismic response." *Earthquake Engineering and Structural Dynamics*, 29(4), 499-521.

[15] Au, F.T.K., Cheng, Y.S., Cheung, Y.K., and Zheng, D.Y. (2001). "On the determination of natural frequencies and mode shapes of cable-stayed bridges." *Applied Mathematical Modelling*, 25(12), 1099-1115.

[16] Caetano, E., Cunha, A., Gattulli, V., and Lepidi, M. (2008). "Cable-deck dynamic interactions at the International Guadiana Bridge: On-site measurements and finite element modelling." *Structural Control and Health Monitoring*, 15(3), 237-264.

[17] Liu, M.Y., Zuo, D., and Jones, N.P. (2005). "Deck-induced stay cable vibrations: Field observations and analytical model." *Proceedings of the Sixth International Symposium on Cable Dynamics*, 175-182, Charleston, South Carolina, USA, September 19-22.

[18] Wang, P.H., Tseng, T.C., and Yang, C.G. (1993). "Initial shape of cable-stayed bridges." *Computers and Structures*, 46(6), 1095-1106.

[19] Wang, P.H., and Yang, C.G. (1996). "Parametric studies on cable-stayed bridges." *Computers and Structures*, 60(2), 243-260.

[20] Wang, P.H., Lin, H.T., and Tang, T.Y. (2002). "Study on nonlinear analysis of a highly redundant cable-stayed bridge." *Computers and Structures*, 80(2), 165-182.

[21] Wang, P.H., Tang, T.Y., and Zheng, H.N. (2004). "Analysis of cable-stayed bridges during construction by cantilever methods." *Computers and Structures*, 82(4-5), 329-346.

[22] Wang, P.H., Liu, M.Y., Huang, Y.T., and Lin, L.C. (2010). "Influence of lateral motion of cable stays on cable-stayed bridges." *Structural Engineering and Mechanics*, 34(6), 719-738.

[23] Liu, M.Y., Lin, L.C., and Wang, P.H. (2011). "Dynamic characteristics of the Kao Ping Hsi Bridge under seismic loading with focus on cable simulation." *International Journal of Structural Stability and Dynamics*, 11(6), 1179-1199.

[24] Liu, M.Y., Zuo, D., and Jones, N.P. "Analytical and numerical study of deck-stay interaction in a cable-stayed bridge in the context of field observations." *Journal of Engineering Mechanics*, *ASCE*. (under review).

[25] Ernst, H.J. (1965). "Der E-modul von Seilen unter Berücksichtigung des Durchhanges." *Der Bauingenieur*, 40(2), 52-55. (in German).

[26] Fleming, J.F. (1979). "Nonlinear static analysis of cable-stayed bridge structures." *Computers and Structures*, 10(4), 621-635.
[27] Newmark, N.M. (1959). "A method of computation for structural dynamics." *Journal of the Engineering Mechanics Division*, *ASCE*, 85(EM3), 67-94.
[28] Cheng, W.L. (2001). "Kao Ping Hsi Bridge." Taiwan Area National Expressway Engineering Bureau, Ministry of Transportation and Communications, Taipei, Taiwan.
[29] Irvine, H.M. (1981). "Cable structures." MIT Press, Cambridge, Massachusetts, USA.
[30] Lee, W.H.K., Shin, T.C., Kuo, K.W., Chen, K.C., and Wu, C.F. (2001). "CWB free-field strong-motion data from the 21 September Chi-Chi, Taiwan, earthquake." *Bulletin of the Seismological Society of America*, 91(5), 1370-1376.